ACS Catalysis

Research Article

pubs.acs.org/acscatalysis

Framework and Extraframework Tin Sites in Zeolite Beta React Glucose Differently

Ricardo Bermejo-Deval,[†] Rajamani Gounder,[†] and Mark E. Davis*

Chemical Engineering, California Institute of Technology, Pasadena, California 91125, United States

Supporting Information

ABSTRACT: Here, we show that framework tin sites in pure silica zeolite Beta (Sn-Beta) can isomerize glucose to fructose by a Lewis acid-mediated intramolecular hydride shift in aqueous solvent, but not in methanol solvent. Mechanistic studies using isotopically labeled (^{2}H, ^{13}C) glucose reactants show that in methanol, Sn-Beta instead epimerizes glucose to mannose by a Lewis acid-mediated intramolecular carbon shift mechanism known as the Bilik reaction. We also provide evidence that extraframework tin sites located within the hydrophobic channels of zeolite Beta can isomerize glucose to fructose in both water and methanol solvent, but through a base-catalyzed proton-transfer mechanism. SnO_2 particles located at external zeolite crystal surfaces or supported on amorphous silica catalyze isomerization in methanol but not in water, suggesting that contact with bulk water inhibits isomerization at SnO_2 surfaces. ^{119}Sn MAS NMR spectroscopy was used to unambiguously identify framework Sn sites, which give resonances for octahedral Sn (−685 to −700 ppm) in hydrated Sn-Beta that disappear upon dehydration, with the concomitant appearance of resonances for tetrahedral Sn (−425 to −445 ppm). In sharp contrast, spectra of hydrated samples containing extraframework SnO_2 show resonances for octahedral Sn centered at −604 ppm that do not change upon dehydration. These findings demonstrate that aldose−ketose isomerization reactivity on Sn-zeolite samples cannot be ascribed to the presence of framework Sn sites in the absence of isotopic labeling studies. They also indicate that any Sn-zeolite samples that initially convert glucose to fructose, instead of mannose, in methanol solvent contain Sn species that are structurally different from framework Sn centers.

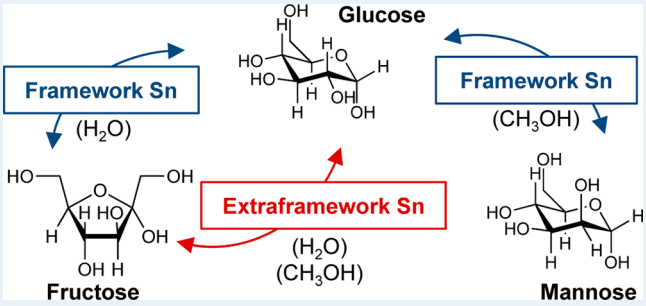

KEYWORDS: *Bilik reaction, epimerization, glucose, isomerization, mannose, methanol, tin-Beta, water*

1. INTRODUCTION

The conversion of molecules containing carbonyl functional groups, notably ring-opened forms of biomass-derived aldose and ketose sugars, using porous solids containing Lewis acidic centers has received considerable attention.[1] Corma et al. initially reported that framework tin centers in zeolite Beta behave as Lewis acids that catalyze the Baeyer−Villiger oxidation and the Meerwein−Ponndorf−Verley (MPV) reduction of carbonyl compounds in organic solvents.[2−4] More recently, Sn and Ti zeolites have been reported to catalyze aldose−ketose isomerization of glucose[5−8] (to fructose) and C_3−C_5 sugars[9,10] in aqueous media. Aldose epimerization products have also been observed with Sn-Beta catalysts for glucose[5,9] (to mannose) and xylose[10] (to lyxose) reactants in aqueous media. The mechanistic details of glucose epimerization on Sn-Beta were not investigated previously, but xylose epimerization to lyxose was proposed to occur via a reversible intramolecular hydride shift that involved an common intermediate with the pathway for xylose isomerization to xylulose.[10] Framework Sn centers in Sn-Beta have also been implicated as active sites that isomerize glucose and other sugars in organic solvents, such as methanol[11−13] and ethanol.[14]

In aqueous media, we have shown previously that framework Sn centers behave as Lewis acids that bind glucose reactants in their acyclic forms and mediate their isomerization to fructose via an intramolecular hydride shift from the C-2 to the C-1 position.[6,8] Glucose reactants containing a deuterium label on the C-2 position (glucose-D2) formed fructose products deuterated in the C-1 position (fructose-D1),[6,8] reflected in ^{13}C NMR spectra that showed low-intensity triplet resonances corresponding to these carbon atoms. Low-intensity resonances in ^{13}C NMR spectra acquired using ^{1}H broadband decoupling reflect the presence of D atoms that disrupt the nuclear Overhauser enhancement (NOE) of ^{13}C resonances via suppression of ^{13}C−^{1}H couplings. The mechanistic evidence obtained from ^{13}C and ^{1}H NMR studies were also consistent with the observed kinetic isotope effect of ∼2 (at 383 K) when using glucose-D2 reactants.[8] Activation energies measured experimentally (89 kJ mol^{-1}) and calculated by MP2-levels of theory for intramolecular hydride shift steps on framework Sn open sites (Sn with three −O(Si) bonds and one −OH group) adjacent to one silanol group (92 kJ mol^{-1}) were also similar.[8] These Lewis acid-mediated isomerization pathways on Sn-Beta in aqueous solvent are analogous to those on metalloenzymes,

Received: July 16, 2012
Revised: October 23, 2012
Published: October 29, 2012

   dx.doi.org/10.1021/cs300474x | ACS Catal. 2012, 2, 2705−2713

such as D-xylose isomerase XI, which contains two divalent metal ions (commonly Mg^{2+} or Mn^{2+}) that facilitate the ring-opening of glucose and the hydride shift from the C-2 to the C-1 positions on the acyclic sugar.[15]

In contrast with the case of glucose isomerization to fructose on framework Sn sites in water, the mechanistic origins of glucose isomerization in methanol and glucose epimerization in either water or methanol remain unclear. Here, we use kinetic and mechanistic studies, focusing on differential glucose conversions and the primary products formed, to distinguish among isomerization and epimerization pathways on framework and extraframework Sn sites in zeolite Beta in both water and methanol. These data show that framework Sn sites behave as Lewis acids that isomerize glucose to fructose in water via intramolecular hydride shifts, but instead epimerize glucose to mannose in methanol via intramolecular carbon shifts. In contrast, extraframework SnO_2 domains located within hydrophobic zeolite Beta channels mediate glucose isomerization to fructose via base-catalyzed proton abstraction in both water and methanol. Extraframework SnO_2 particles located on external zeolite surfaces or on amorphous supports, however, isomerize glucose to fructose in methanol but not in water. These findings help clarify differences in reactivity among Sn sites of different structure and among extraframework SnO_2 particles of different locations within porous solids. They also provide evidence for the mechanism of glucose epimerization to mannose with framework Sn-Beta and for a new pathway for glucose isomerization to fructose with Sn-containing silicates in methanol solvent.

2. EXPERIMENTAL METHODS

2.1. Synthesis of Si-Beta, Sn-Beta, SnO_2/Si-Beta, and SnO_2−SiO_2. Si-Beta was prepared by adding 10.01 g of tetraethylammonium flouride dihydrate (Sigma-Aldrich, 97% (w/w) purity) to 10 g of water and 4.947 g of tetraethylorthosilicate (Sigma-Aldrich, 98% (w/w)). This mixture was stirred overnight at room temperature in a closed vessel to ensure complete hydrolysis of the tetraethylorthosilicate. The targeted H_2O/SiO_2 ratio was reached by complete evaporation of the ethanol and partial evaporation of the water. The final molar composition of the gel was SiO_2/0.55 TEAF/7.25 H_2O. The gel was transferred to a Teflon-lined stainless steel autoclave and heated at 413 K in a rotation oven (60 rpm) for 7 days. The solids were recovered by filtration, washed extensively with water, and dried at 373 K overnight. The dried solids were calcined in flowing air (1.67 cm^3 s^{-1}, Air Liquide, breathing grade) at 853 K (0.0167 K s^{-1}) for 10 h to remove the organic content located in the crystalline material.

Sn-Beta was synthesized according to previously reported procedures.[8] A 7.57 g portion of tetraethylammonium hydroxide solution (Sigma-Aldrich, 35% (w/w) in water) was added to 7.011 g of tetraethylorthosilicate (Sigma-Aldrich, 98% (w/w)), followed by the addition of 0.121 g of tin(IV) chloride pentahydrate (Sigma-Aldrich, 98% (w/w)). The mixture was stirred until tetraethylorthosilicate was completely hydrolyzed and then allowed to reach the targeted H_2O/SiO_2 ratio by complete evaporation of ethanol and partial evaporation of water. Finally, 0.690 g of HF solution (Mallinckrodt, 52% (w/w) in water) was added, resulting in the formation of a thick gel. The final molar composition of the gel was 1 SiO_2/0.01 $SnCl_4$/0.55 TEAOH/0.54 HF/7.52 H_2O. Si-Beta was added as seed material (5 wt % of SiO_2 in gel) to this gel and mixed. The final gel was transferred to a Teflon-lined stainless steel autoclave and heated at 413 K in a static oven for 40 days. The solids were recovered, washed, dried, and calcined using the procedure described above for Si-Beta.

Si-Beta containing extraframework SnO_2 (SnO_2/Si-Beta) was prepared using the same procedure as Sn-Beta, but with substitution of tin(IV) chloride pentahydrate with 0.052 g of tin(IV) dioxide (Sigma-Aldrich, −325 mesh; aggregate particle size <44 μm) as the source of tin in the synthesis gel. The gel was transferred to a Teflon-lined stainless steel autoclave and heated at 413 K in a static oven for 25 days. The recovered solids were washed, dried, and calcined using the same procedure as for Si-Beta and Sn-Beta.

Si-Beta containing extraframework SnO_2 particles located on external crystallite surfaces (SnO_2/Si-Beta-E) was synthesized by first adding 0.059 g of tin(IV) chloride pentahydrate (Sigma-Aldrich, 98% (w/w)) to 10 g of water. This solution was stirred with 1.0 g of Si-Beta in its as-made form for 16 h at ambient temperature. The solids were recovered by centrifugation and dried at 373 K overnight. Finally, the dried solids were calcined in flowing air (1.67 cm^3 s^{-1}, Air Liquide, breathing grade) at 853 K (0.0167 K s^{-1}) for 10 h.

SnO_2 was dispersed on silica (SnO_2/SiO_2) by first adding 0.5 g of tin(IV) chloride pentahydrate (Sigma-Aldrich, 98% (w/w)) to 30 g of water. Two grams of fumed silica (Sigma-Aldrich, 0.2−0.3 mm average particle size) was added to the mixture and stirred for 24 h at room temperature. The solids were recovered, washed, dried, and calcined using the same procedure as for crystalline zeolites.

2.2. Characterization Methods. Atomic Si and Sn contents were determined using a JEOL 8200 electron microprobe operated at 15 kV and 25 nA in a focused beam mode with a 40 μm spot size. Scanning electron microscopy (SEM) images were recorded on a LEO 1550 VP field emission SEM at an electron high tension of 10 kV on zeolite samples after sputtering with carbon to minimize the effects of charging. The crystalline structures of zeolite samples were determined from powder X-ray diffraction (XRD) patterns collected using a Rigaku Miniflex II diffractometer and Cu Kα radiation. Diffuse reflectance UV−visible (DRUV) spectra were recorded using a Cary 3G spectrophotometer equipped with a diffuse reflectance cell; zeolite samples were calcined in air at 853 K for 10 h and exposed to ambient conditions prior to acquiring spectra.

N_2 adsorption isotherms at 77 K were obtained using a Quantachrome Autosorb iQ automated gas sorption analyzer. Zeolite samples (typically 0.03−0.04 g) were pelleted and sieved to retain 150−600 μm particles. Samples were degassed at 353 K (0.167 K s^{-1}) for 1 h, 393 K (0.167 K s^{-1}) for 3 h and 623 K (0.167 K s^{-1}) for 8 h prior to recording dry sample weight. N_2 uptake was recorded between relative pressures of 10^{-7} and 1 at 77 K. Total micropore volumes were estimated from linear extrapolation of mesopore N_2 uptakes to zero pressure and the density of liquid nitrogen (section S.3 of the Supporting Information).

Solid-state magic angle spinning nuclear magnetic resonance (MAS NMR) spectra were recorded using a Bruker Avance 500 MHz spectrometer equipped with a 11.7 T magnet and a Bruker 4 mm MAS probe. Powdered samples (0.06−0.08 g) were packed into 4 mm ZrO_2 rotors with Kel-F caps and spun at 14 kHz. ^{119}Sn NMR spectra were recorded at an operating frequency of 186.5 MHz and were referenced to $(CH_3)_4Sn$. Unless otherwise specified, spectra were acquired on hydrated samples, which were exposed to ambient conditions after calcination in flowing air at 853 K but prior to packing NMR

dx.doi.org/10.1021/cs300474x | ACS Catal. 2012, 2, 2705−2713

Table 1. Site and Structural Characterization of Samples Used in This Study

catalyst	Si/Sn[b]	N_2 micropore volume[c] ($cm^3\ g^{-1}$)	^{119}Sn MAS NMR resonances[a] (ppm) hydrated	^{119}Sn MAS NMR resonances[a] (ppm) dehydrated	UV−visible band centers[d] (nm)
Sn-Beta	87	0.20	−688, −700	−424, −443	203
SnO_2/Si-Beta	92	0.12	−604		280
SnO_2/Si-Beta-E	116	0.20	−606	−602	238
SnO_2/SiO_2	13		−605		247
SnO_2			−604		276
Si-Beta		0.19			n.d.[e]

[a]Relative to $(CH_3)_4Sn$. [b]Determined by electron microprobe. [c]Determined by extrapolation of mesopore N_2 uptakes to zero pressure (Section S.3, Supporting Information). [d]Diffuse reflectance spectra obtained on materials exposed to ambient conditions. [e]n.d., not detected

rotors. Selected samples were dehydrated by heating the packed NMR rotors to 423 K in vacuum and holding overnight prior to acquiring NMR spectra.

Liquid ^{1}H and ^{13}C NMR spectra were recorded using a Varian INOVA 500 MHz spectrometer equipped with an auto-x pfg broad band probe. Proton and carbon chemical shifts are reported relative to the residual solvent signal. ^{1}H NMR spectra were acquired with 256 scans, and ^{13}C NMR spectra were acquired with 1000 scans.

2.3. Reaction Procedures. Reactions with D-glucose (Sigma-Aldrich, ≥99%) were conducted in 10 mL thick-walled glass reactors (VWR) that were heated in a temperature-controlled oil bath placed on top of a digital stirring hot plate (Fisher Scientific). For each catalyst and solvent combination, different metal/glucose molar ratios were used. Reactions on Sn-Beta in water were typically carried out using 1.0 g of a 10% (w/w) glucose solution and a 1:100 Sn/glucose molar ratio. Reactions on Sn-Beta in methanol were typically carried out using 1.0 g of a 1% (w/w) glucose solution and a 1:100 Sn/glucose molar ratio. Reactions on SnO_2/Si-Beta in water and methanol were typically carried out using 1.0 g of a 1% (w/w) glucose solution and a 1:20 Sn/glucose molar ratio. Reactions on SnO_2-SiO_2 were performed using 1.5 g of a 1% (w/w) glucose solution and a 1:10 Sn/glucose molar ratio.

Reactors were placed in the oil bath for specific time intervals and quenched by cooling in an ice bath. Small aliquots were extracted, filtered with 0.2 μm PTFE syringe filter, and mixed with D-mannitol (Sigma-Aldrich, ≥98%) solutions used as an internal standard for quantification (10% (w/w) mannitol for experiments with Sn-Beta in water; 1.5% (w/w) mannitol otherwise). Samples were analyzed by high performance liquid chromatography (HPLC) using an Agilent 1200 system (Agilent) equipped with PDA UV (320 nm) and evaporative light scattering (ELS) detectors. Glucose, fructose, mannose, and mannitol fractions were separated with a Hi-Plex Ca column (6.5 × 300 mm, 8 μm particle size, Agilent) held at 358 K, using ultrapure water as the mobile phase at a flow rate of 0.01 mL s^{-1}. Turnover rates were calculated by normalizing the total moles of glucose converted by the total moles of Sn on each catalyst. For liquid NMR analysis of products formed from isotopic labeling studies using D-glucose-D2 (Cambridge Isotope Laboratories, ≥98%) and D-glucose-^{13}C−C1 (Cambridge Isotope Laboratories, ≥98%), the glucose, mannose, and fructose fractions were separated by HPLC, isolated by evaporation of H_2O, and dissolved in D_2O (Cambridge Isotope Laboratories, 99.9%).

3. RESULTS AND DISCUSSION

3.1. Site and Structural Characterization of Sn-Containing Samples. The X-ray diffractograms of Si-Beta, Sn-Beta, SnO_2/Si-Beta and SnO_2/Si-Beta-E (Supporting Information Figure S.1) showed patterns that were consistent with the zeolite Beta structure, whereas the XRD pattern of SnO_2/SiO_2 (Supporting Information Figure S.1) was consistent with that of an amorphous solid. The XRD pattern of SnO_2/Si-Beta also showed diffraction lines at 2θ values of 26.7° and 34.0° that are characteristic of bulk SnO_2 (Supporting Information Figure S.1). The presence of some extracrystalline SnO_2 aggregates in the SnO_2/Si-Beta sample (synthesized using SnO_2 as the Sn source) indicates that bulk SnO_2 did not completely dissolve or decompose under the hydrothermal conditions used in the synthesis of SnO_2/Si-Beta. The absence of large SnO_2 domains (as detectable by XRD) in Sn-Beta and SnO_2/Si-Beta-E indicates that mononuclear $SnCl_4$ precursors did not aggregate significantly during hydrothermal synthesis of Sn-Beta or during the aqueous-phase exchange and subsequent air treatment (853 K) protocols used to synthesize SnO_2/Si-Beta-E. Indeed, SEM images of the SnO_2/Si-Beta sample, but not of Sn-Beta, showed the presence of large SnO_2 particles (Supporting Information Figure S.2).

Total micropore volumes determined from N_2 adsorption isotherms (Supporting Information Figures S.3−S.6) are 0.20 and 0.19 $cm^3\ g^{-1}$ for Sn-Beta and Si-Beta, respectively (Table 1). The micropore volume for SnO_2/Si-Beta-E, a sample in which SnO_2 was deliberately deposited on the exterior surfaces of Beta crystallites, is also 0.20 $cm^3\ g^{-1}$ (Table 1), consistent with its low Sn content (2.1 wt %) and the absence of any intracrystalline SnO_2 species that may occlude pore volume. In contrast, the micropore volume is 0.12 $cm^3\ g^{-1}$ for SnO_2/Si-Beta (Table 1), which is significantly lower than expected if SnO_2 were present as extracrystalline phases or located within intracystralline voids but only occluding space (~0.18 $cm^3\ g^{-1}$; Section S.2, Supporting Information). These data suggest that SnO_2 domains located at external crystal surfaces and within the pores of SnO_2/Si-Beta prevent access to a fraction of the internal void space in SnO_2/Si-Beta crystals.

^{119}Sn NMR spectra of Sn-Beta after calcination and exposure to ambient conditions (hydrated) show main resonances centered at −688 and −700 ppm (Figure 1a). After dehydration, these resonances disappeared, and new resonances appeared concomitantly at −424 and −443 ppm (Figure 1b), which have been assigned to framework Sn open sites (three framework −O(Si) bonds and one (OH) group) and framework Sn closed sites (four framework −O(Si) bonds), respectively.[8] The ^{119}Sn NMR spectrum of hydrated SnO_2/SiO_2 (Figure 1c) and SnO_2/Si-Beta-E (Figure 1d) samples showed very broad resonances centered near −604 ppm that did not change upon dehydration (dehydrated SnO_2/Si-Beta-E; Figure 1e). The position of these resonances is consistent with the chemical shift of octahedrally coordinated Sn in bulk SnO_2

dx.doi.org/10.1021/cs300474x | ACS Catal. 2012, 2, 2705−2713

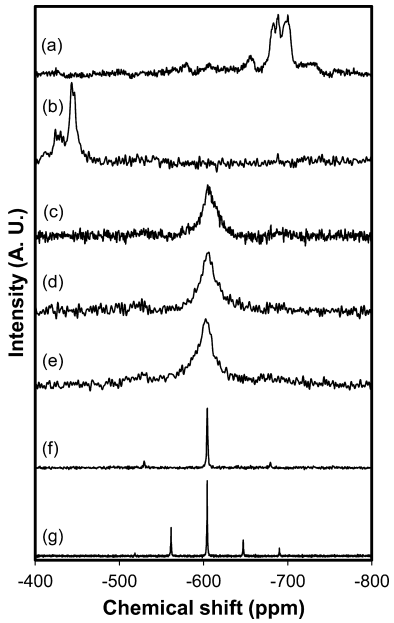

Figure 1. ^{119}Sn MAS NMR spectra of (a) Sn-Beta (hydrated), (b) Sn-Beta (dehydrated), (c) SnO_2/SiO_2 (hydrated), (d) SnO_2/Si-Beta-E (hydrated), (e) SnO_2/Si-Beta-E (dehydrated), (f) SnO_2/Si-Beta (hydrated), and (g) bulk SnO_2 (hydrated).

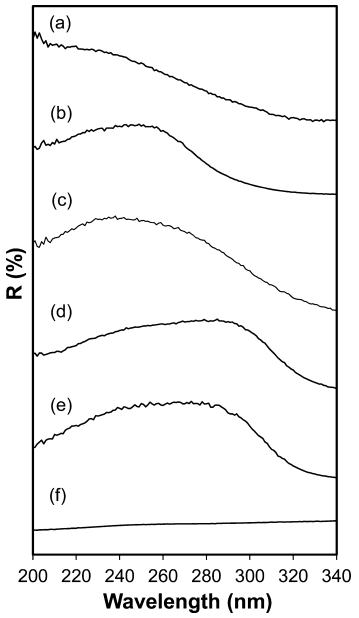

Figure 2. Diffuse reflectance UV−visible spectra of (a) Sn-Beta, (b) SnO_2/SiO_2, (c) SnO_2/Si-Beta-E, (d) SnO_2/Si-Beta, (e) bulk SnO_2, and (f) Si-Beta.

(−604.3 ppm; Figure 1g), and their breadth reflects geometric heterogeneities among the octahedral Sn centers in these samples, as expected from the formation of small SnO_2 domains from mononuclear $SnCl_4$ precursors. In contrast with SnO_2/Si-Beta-E and SnO_2/SiO_2, the ^{119}Sn NMR spectrum of hydrated SnO_2/Si-Beta (Figure 1f) showed a very sharp resonance at −604 ppm. This sharp resonance reflects the presence of large SnO_2 aggregates on SnO_2/Si-Beta, consistent with the diffraction lines for bulk SnO_2 that appear in its XRD pattern (Supporting Information Figure S.1) and the large SnO_2 particles detected by SEM imaging (Figure S.2).

The DRUV spectrum of Sn-Beta (Figure 2a) showed a peak centered at 203 nm (Table 1) that has previously been assigned to tetrahedrally coordinated framework Sn,[5,16] whereas no features were observed in the spectrum of Si-Beta (Figure 2f). The DRUV spectra of SnO_2/SiO_2 (Figure 2b) and SnO_2/Si-Beta-E (Figure 2c) showed peaks centered at 247 and 238 nm (Table 1), respectively, which have been assigned previously to SnO_2 species;[17−20] yet, they also fall in a range (200−260 nm) assigned to Sn centers in silicate frameworks that interact with basic molecules (e.g., H_2O, $(CH_3)CO$, CH_3CN, CH_3OH).[16] The DRUV spectra of bulk SnO_2 (Figure 2d) and SnO_2/Si-Beta (Figure 2e) showed very broad bands ranging from 235 to 290 nm with maxima near 280 nm (Table 1), which have been assigned to hexacoordinated polymeric Sn species.[16] Relations between UV−visible absorption wavelengths and the domain sizes of SnO_2 nanoparticles have been well-documented;[17−20] quantum confinement effects cause an increase in the band gap energies (and concomitant decreases in UV−visible absorption wavelengths) of nanoscale semiconducting oxide domains as they decrease in size. These relations would suggest that the lower UV−visible band centers of SnO_2/SiO_2 and SnO_2/Si-Beta-E (relative to bulk SnO_2 and SnO_2/Si-Beta-E) reflect the presence of smaller SnO_2 domains, consistent with the broader SnO_2 resonances in their ^{119}Sn MAS NMR spectra (Figure 1).

Taken together, these characterization data indicate that Sn species are present as framework Sn sites in Sn-Beta, as extraframework SnO_2 particles supported on extracrystalline surfaces of SnO_2/Si-Beta-E or on amorphous surfaces of SnO_2/SiO_2, and as extraframework SnO_2 particles located both outside and within microporous voids of SnO_2/Si-Beta. This analysis shows clearly that seldom-used ^{119}Sn MAS NMR spectroscopy can unambiguously distinguish framework and extraframework Sn sites and can also provide inferences about the sizes of extraframework SnO_2 domains. In contrast with ^{119}Sn MAS NMR spectra, DRUV spectra are used more commonly to characterize Sn structure but require interpretation of spectral features with more ambiguity and imprecision.

3.2. Glucose Conversion on Sn-Beta and SnO_2-Containing Samples in Water. Fructose was formed as the primary product during differential conversion of glucose on both Sn-Beta and SnO_2/Si-Beta in water. Turnover rates (per mole total Sn) were higher on Sn-Beta than on SnO_2/Si-Beta throughout the temperature range studied (343−373 K; see Section S.4, Supporting Information, for all rate data). The apparent activation energy was also higher on Sn-Beta (93 ± 15 kJ mol^{-1}; Table 2) than on SnO_2/Si-Beta (59 ± 6 kJ mol^{-1}; Table 2). Although both Sn-Beta and SnO_2/Si-Beta are able to isomerize glucose to fructose in water, the different structures of framework and extraframework Sn active sites and the large difference in apparent activation energies between them suggest that different isomerization mechanisms prevail on these two sites.

^{1}H and ^{13}C NMR spectroscopies of products formed from the reaction of a 10% (w/w) solution of glucose-D2 over SnO_2/Si-Beta in water (1 h, 373 K) were used to investigate the isomerization mechanism on SnO_2 active sites, as was done previously with Sn-Beta in water.[6] The ^{13}C NMR spectrum of glucose after reaction (Figure 3a) showed resonances at δ = 74.1 and 71.3 ppm for the C-2 positions of β-pyranose and α-pyranose; their low intensity triplets were also present, reflecting the presence of D atoms, which disrupt the NOE

dx.doi.org/10.1021/cs300474x | ACS Catal. 2012, 2, 2705−2713

Table 2. Turnover Rates (373 K) and Apparent Activation Energies (E_{app}) for Glucose Isomerization to Fructose and Glucose Epimerization to Mannose on Sn-Beta, SnO_2/Si-Beta and SnO_2/SiO_2 in H_2O and CH_3OH Solvents

		turnover rate (373 K) ($/10^{-3}$ mol s^{-1} (mol total Sn)$^{-1}$)		E_{app} (kJ mol^{-1})	
catalyst	solvent	fructose	mannose	fructose	mannose
Sn-Beta	H_2O	27.8 ± 5.0	n.d.[a]	93 ± 15	
Sn-Beta	CH_3OH	n.d.[a]	7.4 ± 1.4		70 ± 14
SnO_2/Si-Beta	H_2O	9.7 ± 1.9	n.d.[a]	59 ± 6	
SnO_2/Si-Beta	CH_3OH	16.6 ± 2.3	n.d.[a]	71 ± 15	
SnO_2/SiO_2	H_2O	n.d.[a]	n.d.[a]		
SnO_2/SiO_2	CH_3OH	4.2 ± 0.3	n.d.[a]	102 ± 9	

[a]n.d., not detected.

of ^{13}C resonances. Thus, the resonance at δ = 74.1 ppm reflects the presence of H atoms at some of the glucose C-2 positions, consistent with the low intensity resonances that appear ~δ = 3.1 ppm for H atoms at the C-2 position in the corresponding ^1H NMR spectrum (Supporting Information Figure S.7). These data indicate that the D-label on glucose-D2 underwent isotopic scrambling in the presence of SnO_2/Si-Beta in water, as we have previously observed after reaction of glucose-D2 with aqueous NaOH solutions, but not with Sn-Beta in water (Supporting Information Figure S.8).[6]

The ^{13}C NMR spectrum of fructose products formed from reaction of glucose-D2 with SnO_2/Si-Beta in water (Figure 3c) showed resonances at δ = 63.8 and 62.6 ppm for the C-1 position of β-pyranose and β-furanose, respectively. The absence of low-intensity triplets for these resonances indicates that no deuterium atoms are bonded to fructose C-1 carbon atoms.[6] The corresponding ^1H NMR spectrum (Supporting Information Figure S.9) shows a resonance at δ = 3.45 ppm for H-atoms bonded to fructose C-1 carbons, confirming the absence of deuterium at C-1 carbon atoms. In our previous work,[6] similar NMR results were reported for NaOH-catalyzed glucose-D2 isomerizations. Thus, the current data show that glucose isomerizes on SnO_2 via a proton abstraction mechanism analogous to the homogeneous base catalyst, in which fructose is formed via enolate intermediates generated from the base-catalyzed proton abstraction at the α-carbonyl carbon (C-2) position of glucose.

Glucose isomerization via reversible enolization proceeds in aqueous alkaline media with activation energies that are nearly twice as large (~120 kJ mol^{-1})[21,22] as observed on SnO_2/Si-Beta in water (59 ± 6; Table 2). Lower apparent activation energies than expected (by factors of ~2) on SnO_2/Si-Beta would be consistent with internal mass transfer limitations of the reaction rate (details in the Supporting Information, Section S.6). Glucose isomerization rates and activation energies measured on SnO_2/SiO_2 and SnO_2/Si-Beta-E, for which diffusion to SnO_2 surfaces are not expected to limit rates, were used to assess whether reactions may be transport-limited on SnO_2/Si-Beta. The conversion of 1 wt % glucose in water mixtures remained below detection limits, however, on SnO_2/SiO_2, SnO_2/Si-Beta-E, and bulk SnO_2 (1:50 Sn:glucose molar ratio) after 15 min at 353 K (Table 3) and on SnO_2/SiO_2 (1:5 Sn/glucose molar ratio), even after 1 h at 373 K. These data indicate that bulk water inhibits base-catalyzed glucose isomerization on SnO_2 surfaces. Thus, we suggest that only SnO_2 domains located within hydrophobic zeolite Beta pores, which are protected from contact with bulk liquid water and also present in the SnO_2/Si-Beta sample, can catalyze glucose isomerization in aqueous solvent.

Table 3. Glucose Conversion to Fructose via Base-Catalyzed Isomerization on SnO_2-Containing Samples in H_2O and CH_3OH Solvents[a]

	glucose conversion (%)	
catalyst	H_2O	CH_3OH
SnO_2/Si-Beta	3.0	5.0
SnO_2/Si-Beta-E	n.d.[b]	3.6
SnO_2/SiO_2	n.d.[b]	0.9
SnO_2	n.d.[b]	n.d.[b]

[a]Reaction conditions: 1% (w/w) glucose solutions, 1:50 metal:glucose ratio, 353 K, 15 min. [b]n.d., not detected.

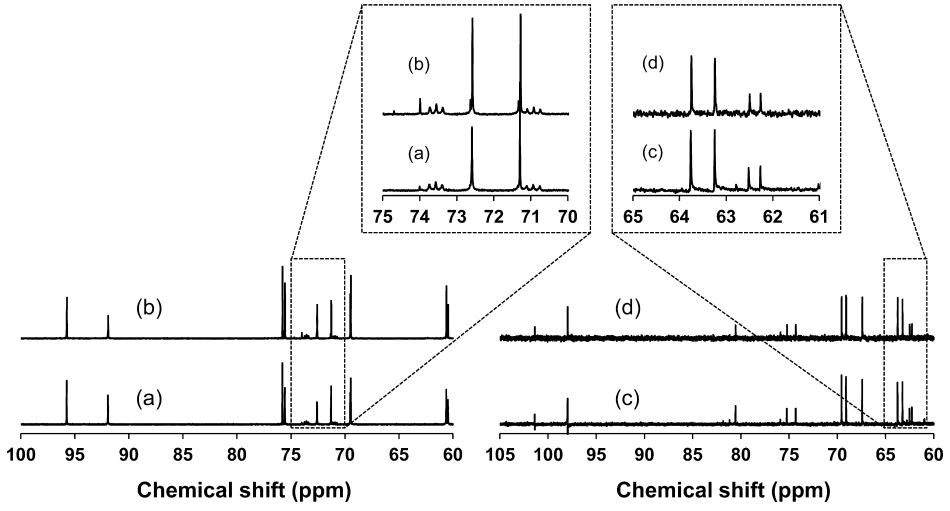

Figure 3. ^{13}C NMR spectra of sugar fractions (glucose or fructose) obtained after reaction of glucose-D2 with SnO_2/Si-Beta in different solvents (water or methanol) at 373 K for 1 h: (a) glucose/water, (b) glucose/methanol, (c) fructose/water, and (d) fructose/methanol.

dx.doi.org/10.1021/cs300474x | ACS Catal. 2012, 2, 2705−2713

3.3. Glucose Conversion on SnO_2-Containing Samples in Methanol. The differential conversion of 1% (w/w) glucose in methanol over SnO_2/Si-Beta formed fructose as the primary product. Turnover rates (per total Sn) were higher (by factors of up to 3; 333−383 K) on SnO_2/Si-Beta in methanol than in aqueous solvent (Supporting Information Table S.1). Glucose also isomerized to fructose on both SnO_2/SiO_2 and SnO_2/Si-Beta-E when methanol was used as the solvent (Table 3), in sharp contrast to the undetectable conversion of glucose on these samples in water under equivalent reaction conditions. These data suggest that contact with bulk methanol does not inhibit isomerization reactivity on SnO_2 surfaces and, in turn, that the higher turnover rates on SnO_2/Si-Beta in methanol than in water (Supporting Information Table S.1) reflect, to an extent, additional contributions from glucose conversion on extracrystalline SnO_2 particles.

In contrast with turnover rates measured over SnO_2/Si-Beta in water, turnover rates over SnO_2/Si-Beta in methanol depended differently on temperature in the 333−363 K and 363−383 K ranges (Figure 4). This behavior may reflect

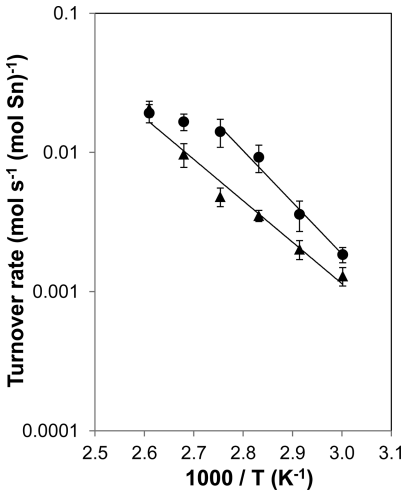

Figure 4. Temperature dependence of turnover rates on SnO_2/Si-Beta for glucose isomerization to fructose in water (triangles) and methanol (circles).

temperature-dependent contributions to measured isomerization rates from SnO_2 particles of different sizes and locations (i.e., extracrystalline or intracrystalline). The apparent activation energy estimated from initial rate data in methanol between 333 and 363 K is 71 ± 15 kJ mol^{-1}, is similar to that determined in water between 343 and 373 K (59 ± 6 kJ mol^{-1}; Table 2). The activation energy for glucose isomerization to fructose on SnO_2/SiO_2 in methanol was 102 ± 9 kJ mol^{-1} (Supporting Information Figure S.10), which is similar to the values of ∼120 kJ mol^{-1} reported for base-catalyzed glucose isomerization in aqueous alkaline media.[21,22] The lower activation energies on SnO_2/Si-Beta in water and in methanol, compared with SnO_2/SiO_2 in methanol, suggest that isomerization rates may, in part, be limited by internal mass transfer restrictions on SnO_2/Si-Beta (section S.6, Supporting Information), as might be expected from the significant decrease in micropore volume accessible to N_2 (∼40%; Table 2).

The mechanism of glucose isomerization on SnO_2/Si-Beta in methanol was probed using ^{13}C and ^{1}H NMR spectroscopies of the products formed from the reaction of glucose-D2 reactants, as in the case of SnO_2/Si-Beta in water. Both ^{13}C (Figure 3b) and ^{1}H NMR (Supporting Information Figure S.11) spectra of the glucose after reaction in methanol provided evidence for H/D scrambling at the C-2 position. Fructose products did not retain the deuterium label on their C-1 positions, as reflected in resonances present at δ = 63.8 and 62.6 ppm in their ^{13}C NMR spectrum (Figure 3d) and at δ = 3.45 ppm in their ^{1}H NMR spectrum (Supporting Information Figure S.12). These spectral features, which reflect the presence or absence of D-atoms at specific carbon atoms in glucose and fructose products, are similar when glucose is reacted with SnO_2/Si-Beta in methanol and in water.

We conclude from these isotopic labeling studies that SnO_2 particles can isomerize glucose to fructose via the base-catalyzed proton abstraction mechanism. Glucose isomerization to fructose on TiO_2 and ZrO_2 particles has been attributed previously to a base-catalyzed mechanism, but solely based on differences in fructose yields and the numbers of basic sites on these catalysts (determined by CO_2 temperature-programmed desorption).[23] Glucose isomerization in methanol occurs irrespective of SnO_2 location within or outside of pore structures, but in water, it apparently requires that SnO_2 domains be confined within hydrophobic microporous channels to prevent their contact with bulk liquid water. Although turnover rates (per total Sn) were larger by factors of ∼3 (333−383 K) on SnO_2/Si-Beta in methanol than in aqueous solvent, the order-of-magnitude higher solubility of glucose in water (∼50 wt %) than in methanol (∼1−2 wt %) implies that significantly higher yields and productivities can be achieved for glucose isomerization in aqueous media.

3.4. Glucose Conversion on Sn-Beta in Methanol. The differential conversion of glucose on Sn-Beta in methanol led to undetectable rates of fructose formation, an unexpected result considering that fructose was formed with high selectivity under analogous conditions on Sn-Beta in water and on SnO_2/Si-Beta in both water and methanol. Reactions of glucose on Sn-Beta in methanol instead formed mannose as a primary product. Turnover rates (per total Sn) for glucose conversion to mannose were factors of ∼4 lower (373 K; Table 2) and apparent activation energies (70 ± 14 kJ mol^{-1}; Figure 5) were ∼23 kJ mol^{-1} lower than those for glucose isomerization to fructose on Sn-Beta in water. Glucose conversion was

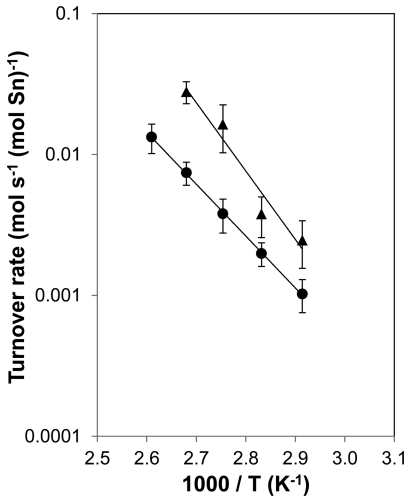

Figure 5. Temperature dependence of turnover rates on Sn-Beta for glucose isomerization to fructose in water (triangles) and epimerization to mannose in methanol (circles).

dx.doi.org/10.1021/cs300474x | ACS Catal. 2012, 2, 2705−2713

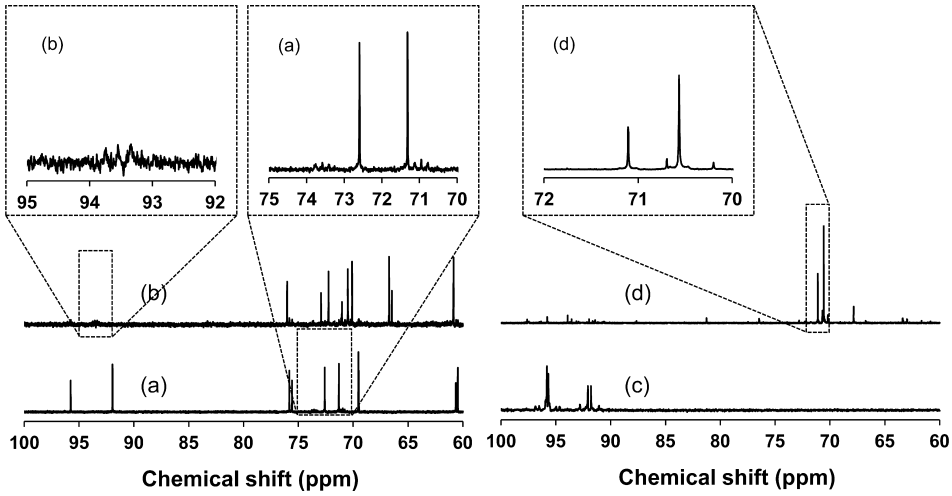

Figure 6. ^{13}C NMR spectra of sugar fractions (glucose or mannose) obtained after reacting different isotopically labeled glucose reactants (glucose-D2 or glucose-^{13}C−C1) with Sn-Beta in methanol at 373 K for 4 h: (a) glucose/glucose-D2, (b) mannose/glucose-D2, (c) glucose/glucose-^{13}C−C1, and (d) mannose/glucose-^{13}C−C1.

undetectable on Si-Beta after 3 h at 373 K (1 g of 1% (w/w) glucose in methanol solution; 0.01 g catalyst), indicating that mannose formation is not due to background reactivity on zeolitic silanol groups or in bulk solution. The formation of mannose as an initial product of glucose conversion requires the presence of framework Sn sites and, apparently, methanol instead of water as the solvent.

Mannose is an epimerization product of glucose that can be formed via reversible enolization (Lobry de Bruyn−Alberda van Ekenstein rearrangements) upon abstraction of α-carbonyl protons or via an intramolecular exchange of carbon atoms at the C-1 and C-2 positions.[24] Glucose reactants labeled with ^{13}C at the C-1 position (glucose-^{13}C−C1) and D at the C-2 position (glucose-D2) would form mannose products with ^{13}C atoms retained at C-1 but without D atoms retained at C-2 if by reversible enolization pathways; however, they would form mannose with ^{13}C and D atoms located at the C-2 and C-1 positions, respectively, if by intramolecular carbon shift steps. Thus, isotopic labeling experiments with glucose-D2 and glucose-^{13}C−C1 reactants with Sn-Beta in methanol were performed following the same procedure as with the other samples, but now with longer reaction times (4 h).

The ^{13}C NMR spectrum of the glucose fraction recovered after reaction of glucose-D2 (Figure 6a) showed only low-intensity triplet resonances at δ = 74.1 and 71.3 ppm at the C-2 positions of glucose, indicating that H/D scrambling did not occur. The mannose fraction collected after glucose-D2 was reacted over Sn-Beta in methanol (Figure 6b) did not show resonances at δ = 93.5 and 93.9 ppm, which correspond to the C-1 positions in α and β pyranose forms of mannose respectively, indicating that deuterium atoms were located at the C-1 positions of mannose. After reaction of glucose-^{13}C−C1 reactants, the glucose fraction (Figure 6c) did not show scrambling of the ^{13}C label, but the mannose products (Figure 6d) showed ^{13}C resonances at δ = 70.5 and 71.1 ppm corresponding to its C-2 positions. This NMR evidence indicates that, in methanol, framework Sn centers epimerize glucose to mannose by intramolecular carbon skeletal rearrangements and not by reversible enolization.

Fructose was observed as a secondary product when glucose was reacted with Sn-Beta in methanol. The ^{13}C NMR spectrum of the fructose products after reaction of glucose-^{13}C−C1 shows the presence of ^{13}C in the C-2 positions (resonances at δ = 98.0 and 101.4 ppm) and the C-1 positions (resonances at δ = 63.8 and 62.6 ppm) of β-pyranose and β-furanose, respectively (Supporting Information Figure S.13). These data suggest that fructose is formed at longer times from glucose (^{13}C label in C-1) and mannose (^{13}C label in C-2), perhaps via enolate intermediates present in minority amounts in solution. In contrast, the ^{13}C NMR spectrum of fructose formed from reactions of glucose-^{13}C−C1 with Sn-Beta in *water* shows ^{13}C located predominantly at C-1 positions (resonances at δ = 63.8 and 62.6 ppm, Supporting Information Figure S.14), consistent with the hydride-shift isomerization mechanism[6] that does not involve carbon scrambling in sugar backbones.

The formation of mannose during differential glucose conversion was observed only in the presence of framework Sn sites and not with extraframework SnO_2, suggesting that the structures of framework Sn active centers are uniquely responsible for epimerization via the carbon shift mechanism. Glucose epimerization was first reported on molybdate anions by Bilik et al.;[25,26] subsequent isotopic labeling and NMR studies by Hayes et al.[27] were consistent with the carbon shift mechanism and showed that reactions of mannose-^{13}C−C1 on molybdate formed exclusively glucose-^{13}C−C2. Lewis acidic metal ion complexes (most notably, Ni^{2+} diamines), as well as alkaline and rare earth ion based complexes, were later reported by Tanase et al.[28−30] and London[31] to also catalyze glucose epimerization to mannose via the carbon shift mechanism. We report here that framework Sn centers in Sn-Beta also behave as Lewis acid sites that epimerize glucose to mannose via carbon skeletal rearrangements in methanol solvent, consistent with their ability to behave as Lewis acids that isomerize glucose to fructose via intramolecular hydride shifts[6,8] in aqueous media.

The similar turnover rates for glucose epimerization in methanol and isomerization in water (within a factor of ~2 at 343−353 K; Supporting Information Table S.1) suggest that both mannose and fructose would have been observed as initial products in either water or methanol solvents if both pathways occurred in parallel. Therefore, the prevalence of epimerization pathways during glucose conversion over Sn-Beta in methanol suggests that methanol, if it could coordinate with framework Sn active sites, may influence the binding of glucose to such

dx.doi.org/10.1021/cs300474x | *ACS Catal.* 2012, 2, 2705−2713

sites or the dynamics of elementary steps required for hydride shift isomerization on such sites. Sn and Ti can expand their coordination from 4-fold to 5- or 6-fold when located in silicate frameworks because they have larger covalent radii than Si.[32] Previous studies have exposed tin silicates to methanol and interpreted changes in DRUV spectra to reflect methanol coordination to framework Sn closed or open sites,[16] whereas methanol coordination with framework Ti centers in Ti-zeolites has been detected using X-ray absorption[33] and in situ UV Raman[34] studies. Although these findings suggest that methanol can interact with framework Sn sites, ongoing work will investigate further the mechanistic roles of methanol in epimerization on framework Sn centers and of water in isomerization on extraframework Sn sites.

4. CONCLUSIONS

In aqueous media, glucose initially undergoes isomerization to fructose on both framework Sn sites and extraframework SnO_2 sites (Scheme 1). Framework Sn centers within the hydrophobic pores of zeolite Beta (Sn-Beta) give ^{119}Sn MAS NMR resonances between −685 and −700 ppm when hydrated but resonances between −425 and −445 ppm when dehydrated. They behave as Lewis acid sites that catalyze isomerization via intramolecular hydride shifts between C-1 and C-2 carbon atoms on acyclic glucose. In contrast, extraframework SnO_2 domains give ^{119}Sn MAS NMR resonances at −604 ppm when hydrated and dehydrated and contain basic sites that catalyze glucose isomerization via the abstraction of protons at C-2 carbon atoms to form enolate intermediates (Scheme 1). Extraframework Sn species appear to be reactive only when confined in hydrophobic zeolite Beta channels (SnO_2/Si-Beta) and not when in contact with bulk water at external zeolite crystal surfaces (SnO_2/Si-Beta-E) and on amorphous supports (SnO_2/SiO_2). These findings demonstrate clearly that the sole observation of glucose-to-fructose isomerization on Sn-zeolite samples, in the absence of isotopic labeling studies and unambiguous methods to characterize Sn structures (e.g., ^{119}Sn MAS NMR spectroscopy), does not provide sufficient evidence for the incorporation of Sn atoms into zeolite frameworks.

Scheme 1. Reaction Network of Glucose with Sn-Beta and SnO_2/Si-Beta in Water and Methanol Solvents[a]

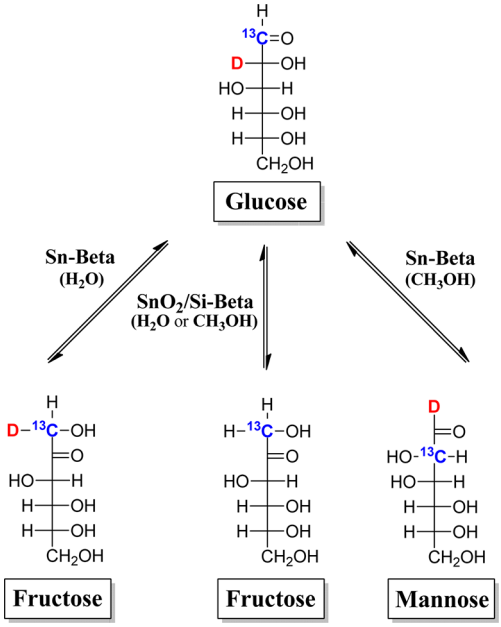

[a]Mechanistic information represented schematically via isotopically-labeled D and ^{13}C atoms in reactants and products. Sugars depicted using Fischer projections.

In methanol solvent, glucose is initially epimerized to mannose on framework Sn sites in Sn-Beta via Lewis-acid-catalyzed intramolecular carbon shifts between its C-1 and C-2 positions (Scheme 1). In contrast, SnO_2 domains isomerize glucose to fructose in methanol via the identical proton-transfer mechanism that prevails on SnO_2 in water (Scheme 1). SnO_2 domains are able catalyze glucose isomerization in methanol irrespective of their location within or outside of hydrophobic zeolite Beta pores, indicating that methanol does not inhibit base-catalyzed isomerization on SnO_2. Although the mechanistic origin of the effects of methanol on the reactivity of framework Sn centers currently remains unclear, its apparent inhibition of isomerization implies that Sn-containing zeolites that initially convert glucose to fructose in methanol solvent do not contain framework Sn species.

■ ASSOCIATED CONTENT

Supporting Information

Catalyst characterization (X-ray diffractograms, SEM images, N_2 adsorption isotherms), reactant and product identification (^{1}H and ^{13}C liquid NMR spectra), and all catalytic rate data are provided. This material is available free of charge via the Internet at http://pubs.acs.org.

■ AUTHOR INFORMATION

Corresponding Author

*E-mail: mdavis@cheme.caltech.edu.

Author Contributions

†R.B.D. and R.G. contributed equally to this work.

Notes

The authors declare no competing financial interest.

■ ACKNOWLEDGMENTS

This work was financially supported as part of the Catalysis Center for Energy Innovation, an Energy Frontier Research Center funded by the U.S. Department of Energy, Office of Science, Office of Basic Energy Sciences under Award No. DE-SC0001004. R.B.D. acknowledges the Obra Social "la Caixa" for a graduate fellowship. We thank Dr. Son-Jong Hwang for the solid-state ^{119}Sn MAS NMR spectra, Dr. David VanderVelde for assistance with the liquid ^{1}H and ^{13}C NMR spectra, Joshua Pacheco for the SEM images, and Carly Bond for experimental assistance with N_2 physisorption measurements.

■ REFERENCES

(1) Román-Leshkov, Y.; Davis, M. E. *ACS Catal.* **2011**, *1*, 1566−1580.
(2) Corma, A.; Nemeth, L. T.; Renz, M.; Valencia, S. *Nature* **2001**, *412*, 423−425.
(3) Corma, A.; Domine, M. E.; Nemeth, L.; Valencia, S. *J. Am. Chem. Soc.* **2002**, *124*, 3194−3195.
(4) Corma, A.; Garcia, H. *Chem. Rev.* **2003**, *103*, 4307−4365.
(5) Moliner, M.; Román-Leshkov, Y.; Davis, M. E. *Proc. Natl. Acad. Sci. U.S.A.* **2010**, *107*, 6164−6168.

(6) Román-Leshkov, Y.; Moliner, M.; Labinger, J. A.; Davis, M. E. *Angew. Chem., Int. Ed.* **2010**, *49*, 8954−8957.
(7) Nikolla, E.; Román-Leshkov, Y.; Moliner, M.; Davis, M. E. *ACS Catal.* **2011**, *1*, 408−410.
(8) Bermejo-Deval, R.; Assary, R. S.; Nikolla, E.; Moliner, M.; Román-Leshkov, Y.; Hwang, S.-J.; Pallsdottir, A.; Silverman, D.; Lobo, R. F.; Curtiss, L. A.; Davis, M. E. *Proc. Natl. Acad. Sci. U.S.A.* **2012**, *109*, 9727−9732.
(9) Lew, C. M.; Rajabbeigi, N.; Tsapatsis, M. *Microporous Mesoporous Mater.* **2012**, *153*, 55−58.
(10) Choudhary, V.; Pinar, A. B.; Sandler, S. I.; Vlachos, D. G.; Lobo, R. F. *ACS Catal.* **2011**, *1*, 1724−1728.
(11) Taarning, E.; Saravanamurugan, S.; Holm, M. S.; Xiong, J. M.; West, R. M.; Christensen, C. H. *ChemSusChem* **2009**, *2*, 625−627.
(12) Holm, M. S.; Saravanamurugan, S.; Taarning, E. *Science* **2010**, *328*, 602−605.
(13) Osmundsen, C. M.; Holm, M. S.; Dahl, S.; Taarning, E. *Proc. R. Soc. A* **2012**, *468*, 2000−2016.
(14) Lew, C. M.; Rajabbeigi, N.; Tsapatsis, M. *Ind. Eng. Chem. Res.* **2012**, *51*, 5364−5366.
(15) Kovalevsky, A. Y.; Hanson, L.; Fisher, S. Z.; Mustyakimov, M.; Mason, S. A.; Forsyth, V. T.; Blakeley, M. P.; Keen, D. A.; Wagner, T.; Carrell, H. L.; Katz, A. K.; Glusker, J. P.; Langan, P. *Structure* **2010**, *18*, 688−699.
(16) Mal, N. K.; Ramaswamy, A. V. *J. Mol. Catal. A: Chem.* **1996**, *105*, 149−158.
(17) Bhagwat, M.; Shah, P.; Ramaswamy, V. *Mater. Lett.* **2003**, *57*, 1604−1611.
(18) Chiodini, N.; Paleari, A.; DiMartino, D.; Spinolo, G. *Appl. Phys. Lett.* **2002**, *81*, 1702−1704.
(19) Gu, F.; Wang, S. F.; Song, C. F.; Lu, M. K.; Qi, Y. X.; Zhou, G. J.; Xu, D.; Yuan, D. R. *Chem. Phys. Lett.* **2003**, *372*, 451−454.
(20) Pang, G. S.; Chen, S. G.; Koltypin, Y.; Zaban, A.; Feng, S. H.; Gedanken, A. *Nano Lett.* **2001**, *1*, 723−726.
(21) Kooyman, C.; Vellenga, K.; Dewilt, H. G. J. *Carbohydr. Res.* **1977**, *54*, 33−44.
(22) Vuorinen, T.; Sjostrom, E. *Carbohydr. Res.* **1982**, *108*, 23−29.
(23) Watanabe, M.; Aizawa, Y.; Iida, T.; Nishimura, R.; Inomata, H. *Appl. Catal., A* **2005**, *295*, 150−156.
(24) Osanai, S. *Top. Curr. Chem.* **2001**, *215*, 43−76.
(25) Bilik, V.; Petrus, L.; Farkas, V. *Chem. Zvesti* **1975**, *29*, 690−696.
(26) Bilik, V.; Petrus, L.; Zemek, J. *Chem. Zvesti* **1978**, *32*, 242−251.
(27) Hayes, M. L.; Pennings, N. J.; Serianni, A. S.; Barker, R. *J. Am. Chem. Soc.* **1982**, *104*, 6764−6769.
(28) Tanase, T.; Shimizu, F.; Kuse, M.; Yano, S.; Yoshikawa, S.; Hidai, M. *J. Chem. Soc., Chem. Commun.* **1987**, 659−661.
(29) Tanase, T.; Shimizu, F.; Kuse, M.; Yano, S.; Hidai, M.; Yoshikawa, S. *Inorg. Chem.* **1988**, *27*, 4085−4094.
(30) Tanase, T.; Shimizu, F.; Yano, S.; Yoshikawa, S. *J. Chem. Soc., Chem. Commun.* **1986**, 1001−1003.
(31) London, R. E. *J. Chem. Soc., Chem. Commun.* **1987**, 661−662.
(32) Camblor, M. A.; Corma, A.; Perez-Pariente, J. *Zeolites* **1993**, *13*, 82−87.
(33) Davis, R. J.; Liu, Z.; Tabora, J. E.; Wieland, W. S. *Catal. Lett.* **1995**, *34*, 101−113.
(34) Wang, L. L.; Xiong, G.; Su, J.; Li, P.; Guo, H. C. *J. Phys. Chem. C* **2012**, *116*, 9122−9131.